

# Comparing the Dynamics of Free Subduction in Cartesian and Spherical Domains

Fangqin Chen<sup>1</sup>, D. Rhodri Davies<sup>1</sup>, Saskia Goes<sup>2</sup>, Lior Suchoy<sup>2</sup>, and Stephan C Kramer<sup>2</sup>

<sup>1</sup>Australian National University

<sup>2</sup>Imperial College London

January 20, 2023

## Abstract

The effects of sphericity are regularly neglected in numerical and laboratory studies that examine the factors controlling subduction dynamics. Most existing studies have been executed in a Cartesian domain, with the small number of simulations undertaken in a spherical shell incorporating plates with an oversimplified rheology, limiting their applicability. Here, we simulate free-subduction of composite visco-plastic plates in 3-D Cartesian and spherical shell domains, to examine the role of sphericity in dictating the dynamics of subduction, and highlight the limitations of Cartesian models. We identify two irreconcilable differences between Cartesian and spherical models, which limit the suitability of Cartesian-based studies: (i) the presence of sidewall boundaries in Cartesian models, which modify the flow regime; and (ii) the reduction of space with depth in spherical shells, alongside the radial gravity direction, which cannot be captured in Cartesian domains. Although Cartesian models generally predict comparable subduction regimes and slab morphologies to their spherical counterparts, there are significant quantitative discrepancies. We find that simulations in Cartesian domains that exceed Earth's dimensions overestimate trench retreat. Conversely, due to boundary effects, simulations in smaller Cartesian domains overestimate the variation of trench curvature driven by plate width. Importantly, spherical models consistently predict higher sinking velocities and a reduction in slab width with depth, particularly for wider subduction systems, enhancing along-strike slab buckling and trench curvature. Results imply that sphericity must be considered when simulating Earth's subduction systems, and that it is essential for accurately predicting the dynamics of subduction zones of width  $\sim 2400$  km or more.

# Comparing the Dynamics of Free Subduction in Cartesian and Spherical Domains

Fangqin Chen<sup>1</sup>, D. Rhodri Davies<sup>1</sup>, Saskia Goes<sup>2</sup>,  
Lior Suchoy<sup>2</sup>, Stephan C. Kramer<sup>2</sup>

<sup>1</sup>Research School of Earth Sciences, The Australian National University, Canberra, ACT, Australia

<sup>2</sup>Department of Earth Science and Engineering, Imperial College London, London, UK

## Key Points:

- Cartesian models of free subduction are strongly affected by domain size and side-wall boundary conditions.
- The reduction in space with depth on a sphere induces buckling during slab descent, concentrating buoyancy and increasing sinking velocity.
- Spherical models are important for simulating Earth's subduction systems, particularly for slabs of width  $\sim 2400$  km or more.

---

Corresponding author: Fangqin Chen, [Fangqin.Chen@anu.edu.au](mailto:Fangqin.Chen@anu.edu.au)

## Abstract

The effects of sphericity are regularly neglected in numerical and laboratory studies that examine the factors controlling subduction dynamics. Most existing studies have been executed in a Cartesian domain, with the small number of simulations undertaken in a spherical shell incorporating plates with an oversimplified rheology, limiting their applicability. Here, we simulate free-subduction of composite visco-plastic plates in 3-D Cartesian and spherical shell domains, to examine the role of sphericity in dictating the dynamics of subduction, and highlight the limitations of Cartesian models. We identify two irreconcilable differences between Cartesian and spherical models, which limit the suitability of Cartesian-based studies: (i) the presence of sidewall boundaries in Cartesian models, which modify the flow regime; and (ii) the reduction of space with depth in spherical shells, alongside the radial gravity direction, which cannot be captured in Cartesian domains. Although Cartesian models generally predict comparable subduction regimes and slab morphologies to their spherical counterparts, there are significant quantitative discrepancies. We find that simulations in Cartesian domains that exceed Earth's dimensions overestimate trench retreat. Conversely, due to boundary effects, simulations in smaller Cartesian domains overestimate the variation of trench curvature driven by plate width. Importantly, spherical models consistently predict higher sinking velocities and a reduction in slab width with depth, particularly for wider subduction systems, enhancing along-strike slab buckling and trench curvature. Results imply that sphericity must be considered when simulating Earth's subduction systems, and that it is essential for accurately predicting the dynamics of subduction zones of width  $\sim 2400$  km or more.

## Plain Language Summary

Subduction zones delineate tectonic plate boundaries where one plate descends beneath another into the underlying mantle. Subduction is responsible for many of Earth's most distinctive geological features, including mountain belts, volcanic island arcs and deep sea trenches. It has long been recognised that the shape of subduction zones is influenced by Earth's sphericity, but sphericity's importance for other aspects of subduction dynamics remains unclear, as the majority of existing modelling studies have been carried out in (easier to simulate) rectangular computational domains. Here, using subduction models with viscosity laws appropriate to mimic plate-like behaviour, we compare predictions from rectangular and spherical models. We show that because rectangular models cannot capture the reduction in space with increasing depth, they consistently underestimate sinking velocities of the subducting plate, which determine how plate temperatures and strength evolve during sinking. Furthermore, the difference in flow patterns that develop in rectangular and spherical models changes how the subducting plates bend, buckle and migrate. Our models show that the discrepancy between Cartesian and spherical subduction models increases with plate width, indicating that spherical models must be used when examining the dynamics of subduction systems that exceed  $\sim 2400$  km in width.

## 1 Introduction

Subduction is the process where oceanic lithosphere descends into the underlying mantle at a convergent plate boundary, providing the major buoyancy force that drives plate tectonics and mantle convection (e.g., Forsyth & Uyeda, 1975; Lithgow-Bertelloni & Richards, 1998; Stern, 2002). Subduction zones influence a wide range of surface processes, including orogeny, the formation of island arcs, the generation and preservation of mineral deposits, and the occurrence of hazardous earthquakes (e.g., Yuan et al., 2000; O'Brien, 2001; Stern, 2002; Rosenbaum et al., 2005; Capitanio et al., 2007; Ishizuka et al., 2011; Wang et al., 2012; Rubey et al., 2017; Perrin et al., 2018; Beall et al., 2021), whilst the descent of subducting slabs also organises underlying mantle flow, modulat-

ing deep mantle structure and the location of upwelling plumes (e.g., Bower et al., 2013; Davies, Goes, & Lau, 2015; Davies, Goes, & Sambridge, 2015; Hassan et al., 2016; Holt & Royden, 2020; Royden & Holt, 2020). Understanding the subduction process is therefore of fundamental importance.

Subduction systems have been studied extensively through both laboratory and numerical approaches, in a Cartesian domain. Several studies have examined how the thermo-chemical structure and material properties of slabs influence the dynamics of subduction and the resulting slab morphology (e.g., Bellahsen et al., 2005; Schmeling et al., 2008; Ribe, 2010; Stegman, Farrington, et al., 2010; Garel et al., 2014; Goes et al., 2017; Mériaux et al., 2018; Suchoy et al., 2021), with many analysing the interaction of slabs with the mantle transition zone (e.g., Čížková et al., 2002; Tagawa et al., 2007; Garel et al., 2014; Agrusta et al., 2017). Cartesian simulations have also been used to examine: (i) the role of slab width in dictating the evolution of subduction systems, particularly the shape and curvature of the trench (e.g., Stegman et al., 2006; Schellart et al., 2007; Stegman, Schellart, & Freeman, 2010; Strak & Schellart, 2016); (ii) the impact of downgoing plate heterogeneities, such as oceanic plateaus and ridges (e.g., Martinod et al., 2005; Mason et al., 2010; van Dinther et al., 2010; Suchoy et al., 2022); and (iii) the importance of an overriding plate (e.g., Jarrard, 1986; Lallemand et al., 2005; Heuret et al., 2007; Capitanio, Stegman, et al., 2010; van Dinther et al., 2010; Garel et al., 2014). These numerical and laboratory studies in an enclosed Cartesian domain provide valuable insight into the sensitivity of subduction to several controlling parameters.

Many of the primary features of Earth’s subduction zones, however, are proposed to be a consequence of our planet’s sphericity. Although not simply the result of slab bending into a sphere, as originally proposed by Frank (1968), arc curvature is likely affected by the spherical shape of the plates and mantle. As slabs descend into the mantle they are squeezed into a smaller area, which is achieved through shortening in the trench-parallel direction, either via slab thickening or buckling (e.g., Scholz & Page, 1970; Strobach, 1973; Laravie, 1975; Bayly, 1982). This has been demonstrated numerically by Fukao et al. (1987) and Yamaoka (1988), who showed that such buckling likely occurs within the stress environment of Earth’s mantle, at a wavelength that depends on the subducting slab’s thickness and its deformable length. This, in turn, will influence the state of stress in the subducting slab, in particular in a trench-parallel direction (Tanimoto, 1998), with radial tears mapped along Wadati-Benioff zones believed to accommodate lateral strains that develop as slabs descend into a spherical shell (e.g., Yamaoka et al., 1986; Cahill & Isacks, 1992; Miller et al., 2006; Schettino & Tassi, 2012). These features demonstrate that the geometric consequences of subduction into a spherical shell are likely significant.

Existing Cartesian based studies have the shortcomings that: (i) they include side boundaries that do not exist in the mantle and, regardless of the thermo-mechanical conditions specified at these boundaries, they will influence the resulting dynamics (e.g., Gurnis & Hager, 1988; Pysklywec et al., 2000; Piromallo et al., 2006; Heuret et al., 2007; Čížková et al., 2007; Stegman, Farrington, et al., 2010; Duretz et al., 2011; Quinquis et al., 2011; Holt et al., 2017); (ii) gravity acts in the vertical direction, as opposed to the radial direction on Earth; (iii) the top and bottom surfaces of the Cartesian domain have the same surface area, which differs to Earth’s mantle, where space constricts with depth; (iv) the top and bottom surfaces of the Cartesian domain are straight edges, which differs to the curved surfaces that bound Earth’s mantle, the latter potentially increasing the geometric stiffness of slabs (Mahadevan et al., 2010; Schettino & Tassi, 2012); and (v) the curvature of internal interfaces on a sphere reduces the incidence angle when a descending slab interacts with the transition zone, potentially enhancing slab stagnation and trench retreat (e.g., Christensen, 2001; Torii & Yoshioka, 2007; Tagawa et al., 2007; Ribe, 2010). These key geometrical differences between Cartesian and spherical models are illustrated in Figure 1.



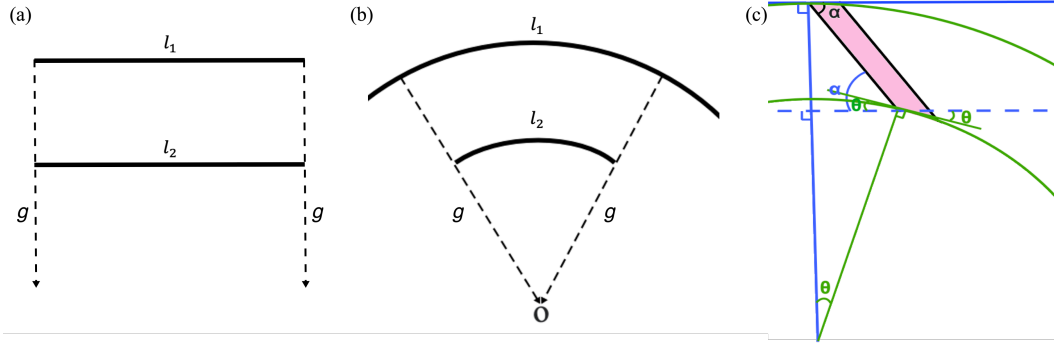


**Figure 1.** Geometrical properties of a spherical shell geometry that may influence the dynamics and evolution of subduction systems, relative to a Cartesian domain: (a) in a Cartesian domain, the direction of gravity,  $g$ , illustrated by dashed arrows, is vertically downwards and parallel across the entire domain. The length  $l_1$  is equal to the length  $l_2$  at depth; (b) the corresponding scenario in a spherical geometry, where material concentrates as it sinks radially towards the centre of the sphere. Bounded by the same radial lines, oriented in the direction of gravity, the length  $l_2$  at depth is shorter than  $l_1$  at the surface. For a 3-D sphere, the tangential area decreases with increasing depth (i.e., the mantle closes in upon itself), requiring slabs to shorten in the trench-parallel direction, either by thickening or buckling (e.g., Strobach, 1973); (c) the curvature of the sphere implies that the dip of a descending slab decreases relative to an internal interface. The example highlighted shows a straight slab of dip  $\alpha$  intersecting the lower mantle in Cartesian and spherical geometries (note, distance not to scale). The slab forms an angle  $\alpha$  with the lower mantle in the Cartesian domain (in blue). In the spherical domain (in green), the tip of the slab traveled an angular distance of  $\theta$  to reach the lower mantle, and forms an angle of  $(\alpha - \theta)$  with the curved interface at the point of intersection. The angular difference ( $\theta$ ) due to the curvature is  $\sim 5^\circ$  for plates with an upper mantle dip ( $\alpha$ ) of  $60^\circ$ . In this study, we test how these differences, and other discrepancies between Cartesian and spherical domains, influence the dynamics and evolution of subduction systems.

Recent studies in Cartesian domains have attempted to reduce the impact of artificial boundaries using open boundary conditions, with only normal flow permitted across sidewalls (e.g., Chertova et al., 2012, 2018). Other studies, using the Boundary Element Method (BEM) (e.g., Pozrikidis, 1992; Morra et al., 2007), have utilised infinite-domain boundary conditions (e.g., Ribe, 2010; Li & Ribe, 2012). However, Earth’s mantle is a spherical shell of finite dimensions, in which convecting cells could ultimately feed back on each other. These feedbacks are constrained by the size of the sphere and will not be captured in simulations with open boundaries or infinite domains. Whilst they can be partially captured through periodic boundary conditions (e.g., Gurnis & Hager, 1988; Han & Gurnis, 1999; Enns et al., 2005; Capitanio, Zlotnik, & Faccenna, 2010; Schellart & Strak, 2021), results will remain sensitive to the dimensions of the domain (e.g., Enns et al., 2005). In light of this, it is important to carefully assess the applicability of Cartesian simulations for investigating the evolution of subduction systems on Earth, which is a goal of this study.

Recently, Morra et al. (2009) used spherical BEM models at the planetary scale to demonstrate that, during subduction, Earth’s sphericity can drive the development of concave curvatures at plate edges and, for wider plates, complex folding at the centre that becomes more pronounced at depth. This is consistent with the postulated role

of Earth’s sphericity and lack of space in inducing slab shortening and buckling. Building on their earlier study, Morra et al. (2012) incorporated a viscosity jump at 660 km depth, demonstrating that slab-transition-zone interaction can further enhance lateral heterogeneity in trench behaviour, with some trench segments partially advancing and others partially retreating, as Earth’s sphericity makes it difficult to maintain plate rigidity for wide plates. Chamolly and Ribe (2021) performed scaling analyses in an axisymmetric shell, validated with BEM simulations, to demonstrate that the effects of sphericity are highly dependent on subducting plate size, suggesting that Earth’s sphericity affects a slab’s trench-parallel normal stress more than its sinking speed. Chamolly and Ribe (2021) attributed the rise of these compressional stresses to the reduction of space during slab descent. Overall, the BEM approach has many advantages over traditional finite element approaches, including increased numerical efficiency. However, there are important limitations, including difficulties in simulating variable viscosity plates. This is a major shortcoming as a growing body of (Cartesian) studies demonstrate that complex plate rheology is fundamental to reproducing the dynamics of subduction on Earth (e.g., OzBench et al., 2008; Capitanio, Stegman, et al., 2010; Stegman, Farrington, et al., 2010; Garel et al., 2014; Király et al., 2017; Alsaif et al., 2020; Cerpa et al., 2022).

In this study, we simulate free subduction of a composite rheology slab in 3-D Cartesian and spherical shell geometries, to examine the role of sphericity in dictating the dynamics of subduction, and to determine when, and under what conditions, the Cartesian approximation of the subduction system breaks down. The paper is structured as follows. We first describe our numerical model setup, and summarise the different cases examined. We subsequently present a systematic quantitative comparison between simulations in Cartesian and spherical shell domains across a broad parameter space. We end by discussing how our results impact any inferences drawn from existing Cartesian studies, in addition to their implications for an improved understanding of the spatial and temporal evolution of subduction zones on Earth.

## 2 Methods

### 2.1 Governing Equations and Numerical Solution Strategy

We follow the approach outlined in Chen et al. (2022). We simulate multi-material free subduction of a composite visco-plastic plate into an ambient mantle, in both 3-D Cartesian and 3-D spherical shell domains, which extend from the surface to a depth of 2890 km. Assuming incompressibility, the governing equations for this problem are the continuity equation

$$\nabla \cdot \mathbf{u} = 0, \quad (1)$$

the conservation of momentum equation for infinite Prandtl number

$$-\nabla p + \nabla \cdot \left[ \mu \left( \nabla \mathbf{u} + (\nabla \mathbf{u})^T \right) \right] = g \Delta \rho \Gamma \hat{k} \quad (2)$$

and an advection equation for composition

$$\frac{\partial \Gamma}{\partial t} + \mathbf{u} \cdot \nabla \Gamma = 0, \quad (3)$$

where  $\mathbf{u}$  is velocity,  $p$  the pressure,  $\mu$  the viscosity,  $\rho$  the density,  $g$  gravity acceleration,  $\hat{k}$  unit vector in the direction opposite gravity, and  $\Gamma$  the material volume fraction ( $\Gamma = 1$  in a region occupied by a given material and  $\Gamma = 0$  elsewhere). The average viscosity is calculated through a geometric mean

$$\mu_{\text{ave}} = \mu_i^{\Gamma_i}, \quad (4)$$

where  $\mu_i$  is the viscosity of material  $i$ , and  $\Gamma_i$  is the relative volume fraction of material  $i$  in the vicinity of the finite-element node at which the effective viscosity  $\mu_{\text{ave}}$  is needed.

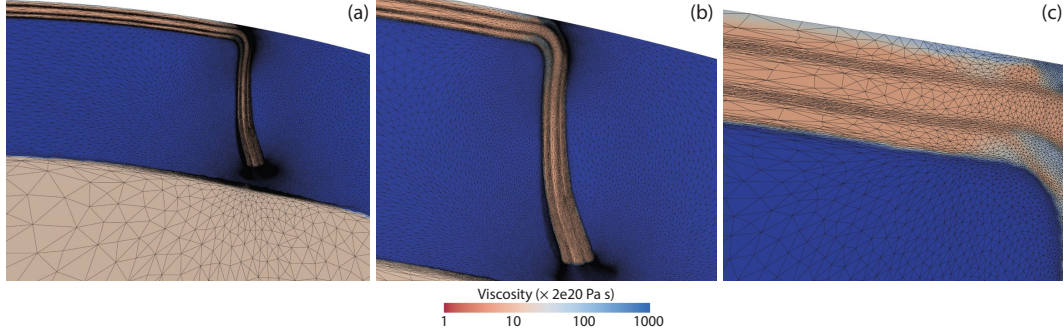


**Figure 2.** Anisotropic adapted unstructured mesh at the symmetry plane from Case S\_W4800, prior to slab interaction with the lower mantle. Each panel focuses on a different region of the domain: (a) a broad region surrounding the slab, illustrating areas of high mesh resolution in regions of dynamic significance (i.e. associated with high curvatures in the velocity and viscosity fields and at the boundary between different materials) – note also the region of high mesh resolution ahead of the slab, facilitated through metric advection, which ensures sufficient resolution in regions of dynamic significance between mesh adapts (e.g., Davies et al., 2011); (b, c) illustrating anisotropic elements that align with material interfaces of the subducting slab, leading to a dramatic reduction in the number of degrees of freedom required for this problem (relative to meshes with isotropic elements), further increasing computational efficiency.

Simulations are carried out using Fluidity (e.g., Davies et al., 2011; Kramer et al., 2012; Davies et al., 2016), a computational modelling framework supporting finite element and control volume discretisations on anisotropic, adaptive, unstructured meshes. Fluidity has been validated for visco-plastic simulations like those examined herein (e.g. Le Voci et al., 2014; Tosi et al., 2015), and for simulations in a spherical shell domain (e.g., Kramer, Davies, & Wilson, 2021). In the context of this study, the framework has several ideal features. Fluidity: (i) can run simulations in 3-D Cartesian and spherical shell domains, using a consistent code base; (ii) uses an anisotropic unstructured mesh, which enables the straightforward representation of complex geometries and materials; (iii) dynamically optimizes this mesh, across parallel processors, providing increased resolution in areas of dynamic importance, thus allowing for accurate simulations across a range of length-scales within a single model; (iv) can employ a free-surface boundary condition, which is important for correctly capturing slab decoupling from the surface (Kramer et al., 2012); (v) utilises the highly-scalable parallel linear system solvers available in PETSc (Balay et al., 1997, 2021a, 2021b), which can efficiently handle sharp, orders of magnitude variations in viscosity; and (vi) has a novel interface-preservation scheme, which allows for the incorporation of distinct materials using volume fractions (Wilson, 2009). In this study, Fluidity’s adaptive mesh capabilities are utilised to provide a local resolution of 3 km in regions of dynamic significance (i.e. at the interface between materials and in regions of strong velocity and viscosity contrasts), with a coarser resolution of up to 300 km elsewhere (Figure 2).

## 2.2 Model Setup

The subducting lithosphere comprises a 2200 km-long composite plate of constant initial thickness ( $h=70$  km) with a core isoviscous layer ( $h_c=30$  km) embedded in upper and lower visco-plastic layers with viscosities that follow a von Mises law, consistent with the reference plate in Chen et al. (2022). Upper and lower visco-plastic layers approx-

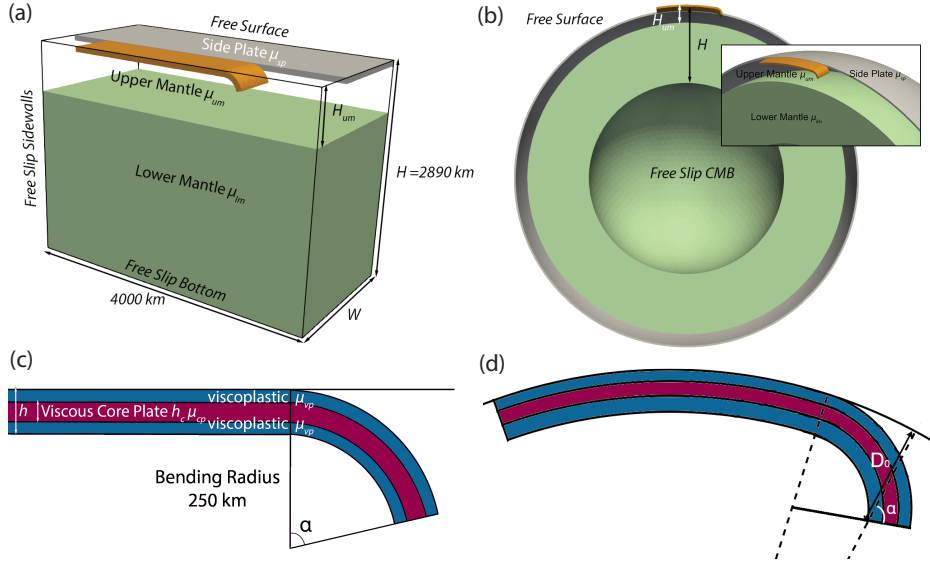


**Figure 3.** Setup of our simulations in: (a) a 3-D Cartesian geometry; and (b) a hemispherical-shell geometry. In both configurations, we exploit the symmetry of the system, halving the computational domain’s extent, whilst bottom and top (inner and outer) boundaries approximate Earth’s core-mantle-boundary and surface, respectively. The side plate is flat in the Cartesian geometry (a), but has a domed shape in the spherical geometry (b), initiated a constant distance from the symmetry plane. (c) Initial slab tip geometry of our layered visco-plastic plates in the Cartesian domain, where the tip is bent an angle of  $\alpha$  with respect to the vertical. (d) Initial slab tip geometry in the spherical shell domain, where the tip is at an angle of  $\alpha$  to the radial direction.

imate the strain-rate weakening that occurs above and below the slab core in thermo-mechanical simulations of subduction (e.g. Garel et al., 2014), following OzBench et al. (2008). Upper and lower layers are assigned the minimum viscosity between the Newtonian viscosity  $\mu_{\text{Newt}}$  and an effective von Mises viscosity  $\mu_{\text{vM}}$ , such that purely viscous deformation occurs as long as the second invariant of the stress tensor  $\tau_{\text{II}} = 2\mu\dot{\epsilon}_{\text{II}}$  (where  $\dot{\epsilon}_{\text{II}}$  is the second invariant of strain rate tensor) does not reach the critical yield stress,  $\tau_{\text{yield}}$ . The effective viscosity of the visco-plastic layers is given by:

$$\mu_{\text{vM}} = \begin{cases} \frac{\tau_{\text{II}}}{2\dot{\epsilon}_{\text{II}}}, & \text{if } \tau < \tau_{\text{yield}} \\ \frac{\tau_{\text{yield}}}{2\dot{\epsilon}_{\text{II}}}, & \text{if } \tau \geq \tau_{\text{yield}} \end{cases} \quad (5)$$

Cartesian models (Figure 3a) have a top surface with a free surface boundary condition and free-slip boundary conditions elsewhere, including the symmetric mid-plane. The gravity direction is vertical. For spherical simulations (Figure 3b), the domain is a hemispherical shell with outer and inner radii that correspond to Earth’s surface and core-mantle boundary (CMB), respectively. The spherical model has a free-surface boundary condition on the outer surface, and a free-slip boundary condition on the symmetry plane and CMB. The gravity direction points radially towards the centre of the sphere.

The subducting plate is surrounded by mantle material, with no overriding or trailing plate. When the plate advances, the mantle material fills in behind the trailing edge. A side plate (dome-shaped in the spherical case) covers the entire domain adjacent to the subducting plate. It has the same thickness as the subducting plate, and is placed

**Table 1.** Parameters common to all simulations examined herein.

Parameter	Symbol	Value
Gravitational acceleration	$g$	10 m/s <sup>2</sup>
Whole plate thickness	$h$	70 km
Core plate thickness	$h_c$	30 km
Characteristic depth (whole mantle)	$H$	2890 km
Depth of upper mantle	$H_{\text{um}}$	660 km
Upper mantle reference viscosity	$\mu_{\text{um}}$	$2.0 \times 10^{20}$ Pa s
Lower mantle reference viscosity	$\mu_{\text{lm}}$	$50 \times \mu_{\text{um}}$
Core plate viscosity	$\mu_{\text{cp}}$	$100 \times \mu_{\text{um}}$
Initial viscosity of visco-plastic layer	$\mu_{\text{Newt}}$	$100 \times \mu_{\text{um}}$
Side plate viscosity	$\mu_{\text{sp}}$	$1000 \times \mu_{\text{um}}$
Yield stress	$\tau_{\text{yield}}$	100 MPa
Mantle density	$\rho$	3300 kg/m <sup>3</sup>
Plate density relative to mantle density	$\Delta\rho$	80 kg/m <sup>3</sup>

225 22 km away from the plate’s edge, keeping a constant distance from the symmetry plane.  
 226 The side plate is 1000 times more viscous than adjacent upper mantle material, and pre-  
 227 vents lateral flow from narrowing the width of downgoing plate (as in Holt et al., 2017).  
 228 The lower mantle is 50 times more viscous than the upper mantle, with the viscosity jump  
 229 at 660 km depth. Model parameters common to all simulations are listed in Table 1.

### 230 2.3 Cases Examined

231 Our models and the parameters explored are listed in Table 2. We examined three  
 232 subducting-plate widths, of 1200 km, 2400 km and 4800 km, in both Cartesian and spher-  
 233 ical domains. For the reference Cartesian simulations, following the setup of Stegman,  
 234 Farrington, et al. (2010), the domain is 4000 km long, 2890 km deep, whilst the width  
 235 ( $W$ ) depends on the width of the plate ( $w$ ) where  $w/W = 0.3$ . In a domain of these  
 236 dimensions, the tail of the plate is 600 km from the edge of the domain. To test the ef-  
 237 fects of Cartesian domain size, we also ran some ‘big’ cases in a domain where we quadru-  
 238 pled the trailing edge distance, the trench distance and the side distance, which denote  
 239 perpendicular distances from the trailing edge, trench, and side of plate to the domain  
 240 boundaries, respectively.

241 The geometrical differences between Cartesian and spherical shell domains leads  
 242 to intrinsic differences in the initial geometry of the subducting plate setup. In our ref-  
 243 erence Cartesian cases, the initial slab tip geometry is prescribed with a bending radius  
 244 of 250 km, terminating at an angle of  $\alpha$  to the vertical direction (Figure 3c), which we  
 245 set to  $77^\circ$  following the setup of Garel et al. (2014). However, if one assumes the same  
 246 angle to the radial direction, the initial slab tip lies deeper in the spherical shell domain  
 247 (Figure 3d). To determine if this difference has a significant impact on results, we have  
 248 also examined two additional cases: (i) a 1200 km-wide Cartesian case where the initial  
 249 slab tip depth is consistent with the spherical cases (C-W1200\_Deep case, with  $\alpha = 83.9^\circ$ );  
 250 and (ii) a 1200 km-wide spherical case where the initial slab tip is shorter and its initial  
 251 depth consistent with Cartesian cases (S-W1200\_Shallow case, with  $\alpha = 63^\circ$ ).

252 With a total of 11 cases, we examine the differences between subduction dynam-  
 253 ics in Cartesian and spherical shell domains for three plate widths, while simultaneously  
 254 exploring the effects of Cartesian domain sizes, and the potential effects of the intrin-  
 255 sic differences in initial conditions arising from the geometric differences between differ-  
 256 ent domain types.

**Table 2.** Simulations examined and associated model parameters. Width refers to full plate width (of which only half is simulated, assuming a central symmetry plane). Trailing Dist., Trench Dist., and Side Dist. represent perpendicular distances from the trailing edge, trench, and side of plate to the domain boundary, respectively. Dip angle refers to the angle to the gravitational direction that the initial slab tip terminates at.

Case	Domain	Width (km)	Trailing Dist. (km)	Trench Dist. (km)	Side Dist. (km)	Dip Angle (°)
C_W1200	Cartesian	1200	600	1200	1400	77
C_W1200_Big	Cartesian	1200	2400	4800	5600	77
C_W1200_Deep	Cartesian	1200	2400	4800	5600	83.9
C_W2400	Cartesian	2400	600	1200	2800	77
C_W2400_Big	Cartesian	2400	2400	4800	11200	77
C_W4800	Cartesian	4800	600	1200	5600	77
C_W4800_Big	Cartesian	4800	2400	4800	22400	77
S_W1200	Spherical	1200	-	-	-	77
S_W1200_Shallow	Spherical	1200	-	-	-	63
S_W2400	Spherical	2400	-	-	-	77
S_W4800	Spherical	4800	-	-	-	77

## 2.4 Model Diagnostics

To quantify how the computational domain’s geometry and size influence results, we have calculated several diagnostic outputs from these models. We define the boundary of the slab as the 0.5 contour of the mantle material volume fraction (material volume fraction = 1 when the material is mantle, 0 otherwise). Based on this contour, we extract the slab tip depth, slab tip width (measured at 100 km above the deepest slab tip depth), and trench location (measured at 15 km depth). We calculate the ratio of trench retreat to the total amount of slab convergence (sum of trench retreat and trailing edge advance). We also trace the evolution of trench geometry relative to the initial trench shape at a depth of 15 km using the slab contour. We extract the maximum sinking velocity in the direction of gravity, both at the symmetry plane and throughout the entire domain. In Cartesian domains, the direction of gravity is always vertical, whereas for spherical models, the direction of gravity is radially towards the centre of the sphere from the point of measurement. All measurements are taken at the symmetry plane, unless otherwise specified.

## 3 Sensitivity to Cartesian Domain Size

We compare predictions from Cartesian simulations for a range of plate widths in two different domain sizes: (i) the reference domain size; and (ii) the ‘Big’ domain.

We find that both trench retreat (Figure 4g-i) and the ratio between trench retreat and total descent (Figure 4j-l) increase in larger Cartesian boxes, which influences the evolution of trench shape. In our reference domain, as plate width increases, the trench evolves from a ‘C’-shape to a ‘W’-shape (an ‘S’-shape when halved at the symmetry plane) with enhanced localised concave curvature close to the trench’s edge, as illustrated in Figure 5. Although the centre of the trench retreats quicker for 1200 km-wide cases in the larger Cartesian domain, the subduction regime remains consistent with its reference domain size equivalent. However, for 4800 km-wide plates, the centre of the trench retreats in the larger domain, but advances in the smaller domain. In other words, this



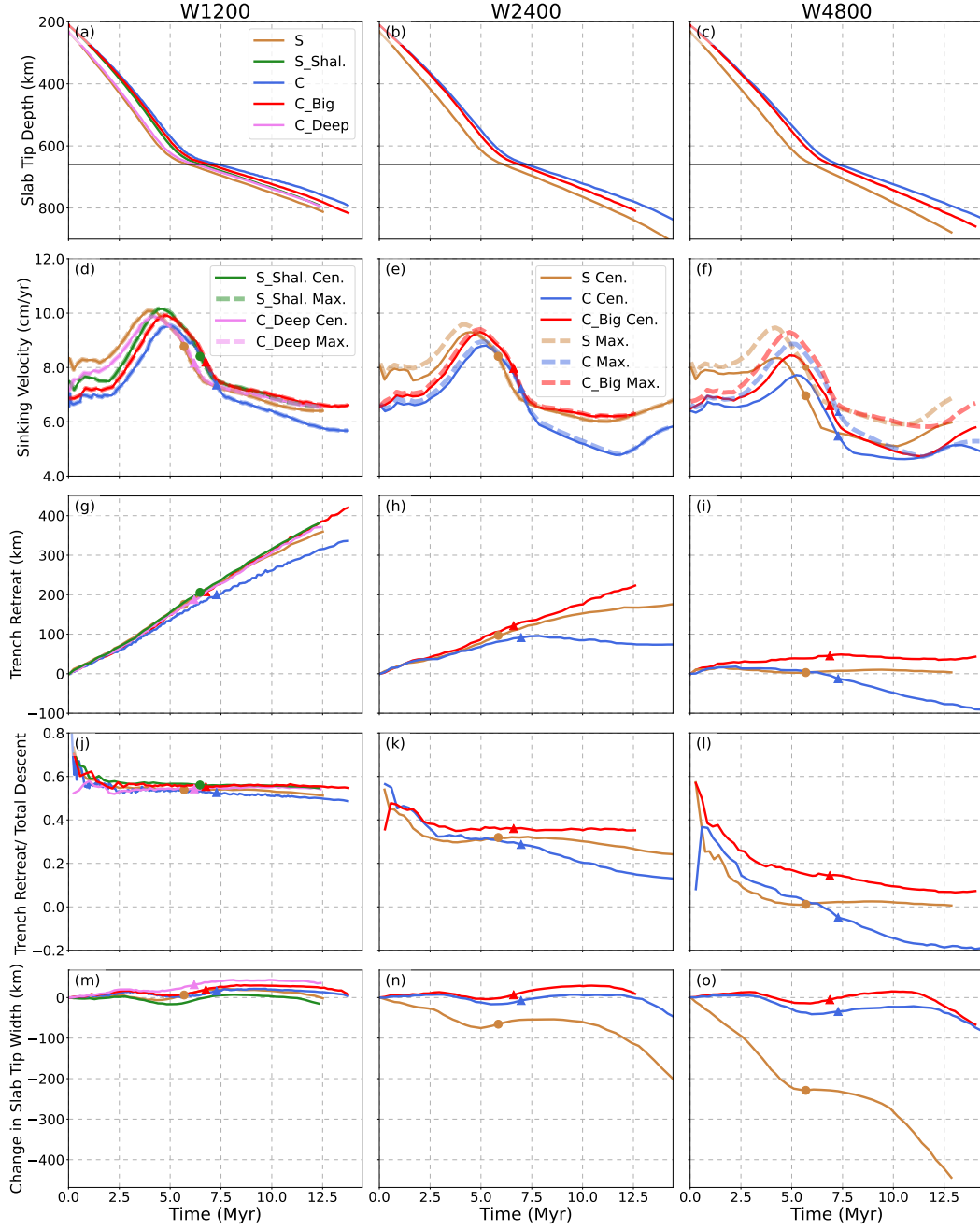


**Figure 4.** Comparison between simulations at plate widths of 1200 km (left column: a,d,g,j,m), 2400 km (central column: b,e,h,k,n) and 4800 km (right column: c,f,i,l,o). (a–c) slab tip depth, as a function of time, where the upper–lower mantle boundary is indicated by the black line at 660 km depth; (d–f) vertical/radial slab sinking velocity at the symmetry plane (Cen.) and the maximum sinking velocity anywhere along the slab (Max.); (g–i) amount of trench retreat; (j–l) ratio of trench retreat to total length of plate subducted, the latter equating to the sum of trench retreat and trailing edge advance; (m–o) change in slab tip width over time, measured 100 km above the slab’s deepest point. In all plots, triangles and filled circles indicate the time where the slab tip first reaches 660 km depth for Cartesian and spherical simulations, respectively. All measurements are taken at the symmetry plane except for the maximum sinking velocity (in d–f) and slab tip width (in m–o). In panel d, the maximum sinking velocities across the entire domain correspond to the sinking velocities at the slab centre, thus results overlap.

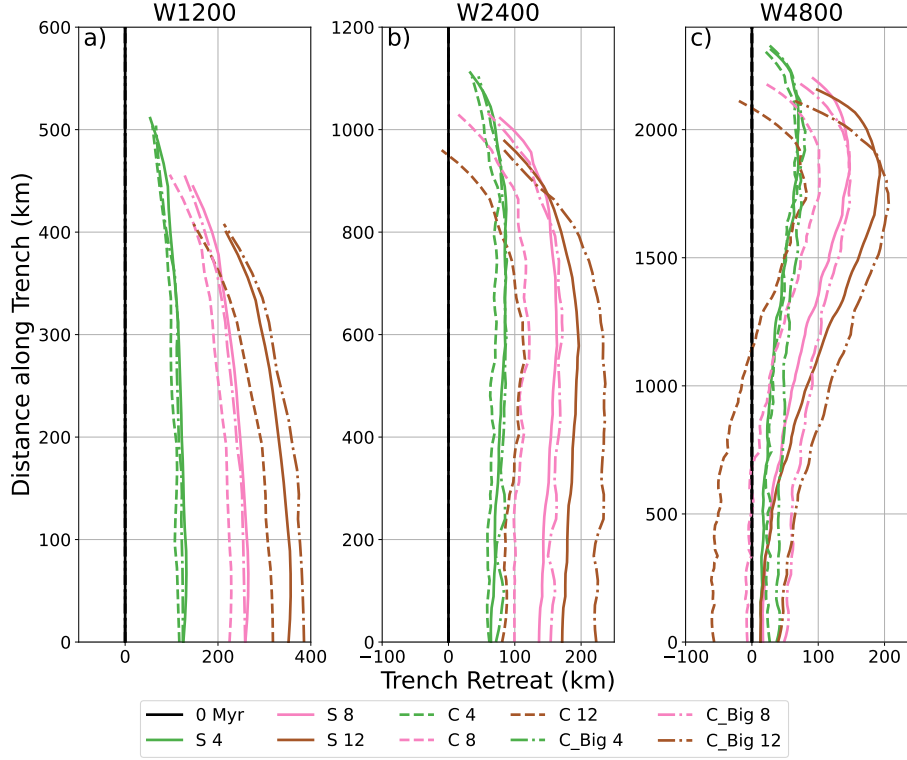


**Figure 5.** Spatio-temporal evolution of trench location for cases with a plate width of: (a) 1200 km; (b) 2400 km; and (c) 4800 km. Numbers in the legend correspond to times in Myr since simulation initiation. S – Spherical; C – Cartesian; C\_Big – ‘Big’ Cartesian domain.

case transitions into a different subduction regime purely through a change in the domain size (Figure 4g,i).

These along-strike variations in trench shape are accompanied by differences in sinking velocities across the slab: for 1200 km-wide cases, maximum sinking velocities are consistent throughout, but for 4800 km-wide cases, the maximum sinking velocity is  $\sim 1$  cm/yr less at the symmetry plane than the overall slab maximum (Figure 4d,f). In general, we find that subducting slabs sink faster in larger Cartesian domains than in smaller domains, as evidenced by both slab tip depths and sinking velocities as a function of time (Figure 4a-f). Although this trend is consistent across all plate widths examined, discrepancies increase with increasing plate width: the difference in maximum sinking velocity at the symmetry plane between simulations in the reference and ‘big’ Cartesian domains increases from  $\sim 0.37$  cm/yr ( $\sim 3.9\%$  of the maximum velocity at the symmetry plane for the reference domain size) for 1200 km-wide slabs to  $\sim 0.73$  cm/yr ( $\sim 9.4\%$ ) for 4800 km-wide slabs (Figure 4d,f; cf. C\_Centre and C\_Big\_Centre). We note that along-strike differences in sinking velocities are reduced in the bigger Cartesian domain. For 4800 km-wide plates, the difference in the maximum sinking velocity across the trench is  $\sim 1.15$  cm/yr ( $\sim 14.9\%$  of the maximum sinking velocity at the symmetry plane) in the reference domain, but only  $\sim 0.85$  cm/yr ( $\sim 10\%$ ) in the bigger domain.

It is noteworthy that discrepancies between Cartesian models in different domain sizes are enhanced upon slab interaction with the more viscous lower mantle at 660 km depth. This is clearly visible in the 2400 km-wide cases, and is also observed for the 4800 km-wide cases, with divergence in a range of diagnostics evident post interaction with the



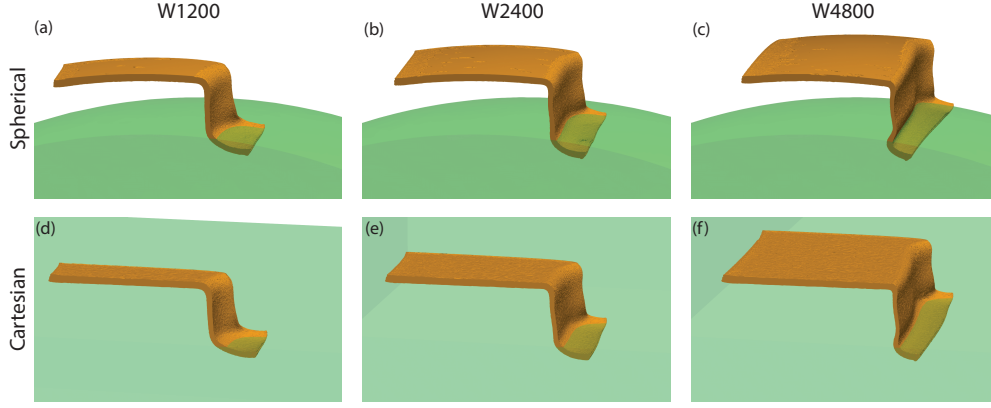


**Figure 6.** 3-D morphology of spherical (top) and Cartesian (bottom) cases, 12 Myr after model initiation, at a plate width of: (a/d) 1200 km; (b/e) 2400 km; (c/f) 4800 km. All Cartesian results shown are from simulations in the ‘Big’ domains.

mantle transition zone. Particularly affected are rates of trench retreat and the trench retreat to total descent ratio (Figure 4h,k). At a width of 2400 km, upon interaction with the lower mantle the slab keeps retreating in the larger domain. Conversely, trench advance occurs at the symmetry plane in the reference domain. Once again, this highlights a transition into a different subduction regime purely as a consequence of a change in domain dimensions (Figure 4i,j).

Taken together, these results provide clear evidence that enforced boundary conditions at domain sidewalls affect the system’s ability to transport material in a regime dominantly dictated by slab and adjacent mantle properties. In smaller domains, the limited space between sidewalls and the subducting slab confines the space through which mantle material can flow around the slab, as suggested in previous studies (e.g., Piromallo et al., 2006; Stegman et al., 2006; Quinquis et al., 2011; Duretz et al., 2011, 2012). Such boundary effects are reduced in larger domains due to an increase in the distance between the slab and side boundaries (e.g., Chertova et al., 2012; Čížková et al., 2012). Trench retreat requires material transport around the slab (e.g., Schellart, 2004; Funiello et al., 2006), which is easier when boundaries are located further from the subduction zone. As trench retreat is enhanced in larger Cartesian domains, slabs expend less energy in bending at the trench (e.g., Capitanio et al., 2007; Goes et al., 2017), particularly at the symmetry plane. Consequently, we also observe increased slab sinking velocities as the domain size increases, and less variation in sinking velocities along the entire slab. We note that the impact of boundary conditions is expected to increase with increasing mantle viscosity (e.g., Piromallo et al., 2006), as the flow field extends over a larger area. This explains the increased discrepancies observed between Cartesian models in different domain sizes post interaction with the higher viscosity lower mantle. Given that boundary effects are reduced in the ‘Big’ domain, in the following sections we mainly compare Cartesian results from these larger cases with their equivalent spherical simulations to isolate the role of sphericity on subduction models.

#### 4 The Role of Sphericity

Models of subduction in a spherical shell better capture the geometry of Earth’s mantle than their Cartesian counterparts. In a reassuring result, we find that spherical shell models generally produce subduction styles and associated slab morphologies that

are similar to their Cartesian equivalents. This is particularly true in the case of narrow slabs, and when comparing to simulations in the larger Cartesian domains. In both spherical and Cartesian simulations, as subduction initiates, the slab tip steepens. During the upper mantle sinking phase, for slabs  $\leq 2400$  km in width, the trench steadily retreats from its initial position, and the plate's trailing edge advances steadily. For 4800 km-wide slabs, however, trench retreat is limited, particularly at the symmetry plane. Accordingly, as subduction matures, we observe increasing along-strike trench curvatures and associated variations in slab morphology with increasing plate width, consistent with predictions from Cartesian models. Across all widths examined, following interaction with the viscosity jump at 660 km depth, the slab tip is deflected, the slab sinking rate reduces substantially, and the upper mantle section of the slab steepens. The slab then slowly sinks into the lower mantle (Figures 5 and 6).

Despite these similarities, there are important discrepancies between spherical and Cartesian model predictions, particularly when comparing trench retreat velocities, the evolution of slab width during slab descent, and slab sinking velocities. Moreover, the significance of such discrepancies increases for wider plates. At the symmetry plane, we find that Cartesian models in the reference and larger domains underestimate and overestimate trench retreat velocities, respectively, when compared to their spherical counterparts. This highlights an important shortcoming of Cartesian simulations: although increasing the box size can allow less restricted material transport around the slab, reducing the impact of side boundaries, Earth's subduction systems are confined by the mantle's dimensions. As a consequence, Cartesian simulations in domains that exceed Earth's dimensions, or those with infinite or open boundaries, fail to capture the complexity of mantle flow generated by subduction in a finite domain, particularly as plates get wider. Although the flow generated by subduction on a sphere does not interact with sidewalls, for a wide plate, the flow field is forced around the sphere and can extend over a large area. Given the domain's finite dimensions and geometry, such flow can ultimately feedback on the dynamics of subduction, limiting the transport of material from the back to the front of a subducting slab (Figure 7). As a consequence, the larger the plate, the harder it is to retreat in a spherical domain, especially at the slab centre. We note that such feedbacks will not be fully captured in Cartesian domains, even with periodic boundaries, as the flow regime in a spherical setting is fully 3-D and not completely periodic (Figure 7).

Due to these factors that hamper the retreat of wide slabs on a sphere, such plates transition more towards a bending mode, particularly at the symmetry plane. As noted previously, such bending means that more energy is expended deforming the slab at its centre, leading to locally lower sinking speeds relative to the plate's edges, and reinforcing along-strike morphological differences. Despite this, we find that spherical models consistently display maximum sinking velocities that exceed their large box Cartesian counterparts (Figure 4d-f), and that these differences generally grow over time. This is significant and contrary to energetic expectations, implying important differences elsewhere between Cartesian and spherical systems.

Our results demonstrate that slabs in spherical models have higher maximum sinking velocities than their Cartesian counterparts (Figure 4d-f). Moreover, we find that these maximum sinking velocities are largely insensitive to initial conditions. We have tested whether the different basal areas of subducting plates (with the same upper surface area) in Cartesian and spherical domains impacts results, given its effect on basal drag. Although not plotted herein, we found that increasing the basal area of spherical models to match the corresponding Cartesian model made little difference to the diagnostic outputs examined. We have also investigated the effect of initial slab tip geometry, through Case C\_W1200\_Deep and Case S\_W1200\_Shallow, and found that whilst the initial tip geometry influences initial slab buoyancy, initial sinking velocity and accordingly strain-rate-dependent viscosity, it has very little influence on the peak sink-

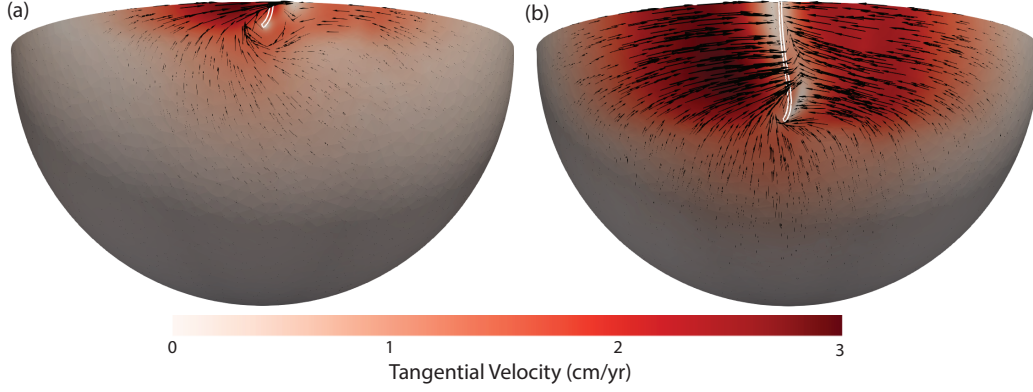


**Figure 7.** Tangential velocities at 300 km depth, 12 Myr after model initiation, for spherical cases: (a) S\_W1200 and (b) S\_W4800. The location of the slab at this depth is outlined in white. Glyphs represent tangential velocity directions and magnitudes, with the largest glyph equating to a magnitude of 3 cm/yr. The maximum tangential velocities for the 1200 km and 4800 km wide spherical cases are 2.7 cm/yr and 3 cm/yr, respectively. Note how the 4800 km wide slab covers a substantial proportion of the distance between the equator and the pole, driving a flow field across the entire hemispherical domain.

ing velocity. In the case of C\_W1200\_Deep, although a deeper initial slab tip increased initial slab sinking velocities compared to case C\_W1200\_Big, velocities do not increase to match those of case S\_W1200 (4d). Our analyses suggest that persistently higher initial sinking velocities in spherical cases arise due to the radial gravity direction on a sphere. As subduction initiates, the slab tip steepens, but requires less bending to align with the radial direction in a spherical domain than with the vertical direction in a Cartesian domain. However, despite the differences in initial sinking velocity, the maximum sinking velocity reached in case C\_W1200\_Deep is comparable to case C\_W1200\_Big with the reference initial tip configuration (Figure 4d), demonstrating that the peak sinking velocity is insensitive to its initial geometry. Likewise, the shorter initial tip in case S\_W1200\_Shallow reduced the initial sinking velocity compared to case S\_W1200, but still reached a similar maximum sinking velocity as S\_W1200, which is much higher than Cartesian model C\_W1200 with similar initial tip depth. This further illustrates that the peak sinking velocity is less sensitive to the initial slab tip configuration than it is to the domain type. Given that spherical models display consistently higher maximum sinking velocities than their Cartesian counterparts (Figure 4d-f), we conclude that the increase in sinking velocity arises due to another aspect of subduction in a spherical domain.

We find that spherical models consistently exhibit a reduction in slab tip width over time (i.e., slab tip narrows in the trench-parallel direction), whereas in Cartesian models, slabs generally maintain their initial width as they descend (Figures 4m-o and 8). For example, in a spherical domain, the 4800 km-wide slab narrows by  $\sim 230$  km prior to interaction with the transition zone. Differences in slab thickness between the spherical and Cartesian models are negligible (not shown), indicating that slabs tend to shorten in the trench-parallel direction by buckling, rather than thickening. Not only does this buckling drive variations in along-strike trench curvature and slab morphology (see Figures 5 and 6), but it also concentrates slab buoyancy, and this, in turn, drives the observed increase in sinking velocities.

We find that discrepancies between Cartesian and spherical models increase with increasing width of the subducting slabs. Over the parameter space examined, quanti-

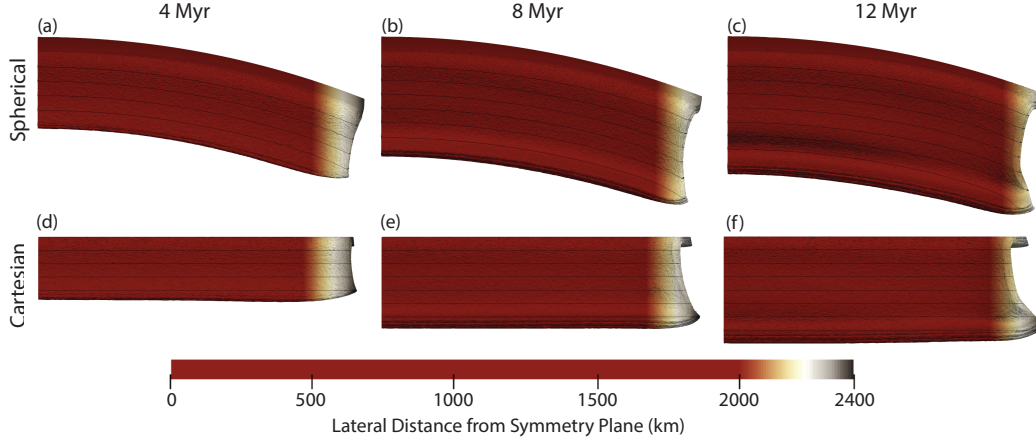


**Figure 8.** Front views of 4800 km-wide slab models, coloured by lateral distance from the symmetry plane, in spherical (top, case S\_W4800) and Cartesian (bottom, case C\_W4800.Big) cases, at simulation times of: (a/d) 4 Myr; (b/e) 8 Myr; and (c/f) 12 Myr, respectively. Slab depth is contoured in 100 km intervals. For the spherical case, slab width reduces with depth, especially during the upper mantle sinking stage, as illustrated in panel a. Over the same period, the width of the deepest part of the slab does not change substantially in the C\_W4800.Big case (d). Upon interaction with the lower mantle at 660 km depth, poloidal flow ceases, and toroidal flow focuses on the upper mantle portions of slabs, enhancing the curvature of slab edges for both spherical (b,c) and Cartesian (e,f) cases.

tative diagnostics begin to diverge at a width of  $\sim 2400$  km. For narrower 1200 km-wide cases, big-domain Cartesian cases predict slab sinking and trench retreat velocities that are in good agreement with their spherical equivalent. At 2400 km width, however, trench retreat at the symmetry plane slows post interaction with the transition zone for the spherical model, while the trench continues to retreat almost unhindered in the bigger Cartesian domain, and the trench advances in the reference domain. Similarly, for 4800 km-wide plates, the centre of the trench stagnates in spherical models, but continues to retreat in the bigger Cartesian domain, and advances in the smaller box. Wider plates in spherical domains also experience more along-strike buckling, manifest in a reduction in slab width as a function of depth (Figure 4m-o), in the evolution of trench curvature (cf. Figure 5 where the maximum retreat distance is similar for Cartesian and spherical models but Cartesian models retreat more at the symmetry plane), and in slab morphologies at depth (Figures 6 and 8).

It is clear, therefore, that the reduction of space with depth in spherical domains induces significant differences in the dynamics of subduction when compared to Cartesian models. To accommodate the shrinking space, slab width reduces with depth through an increase in along-strike buckling (Figure 4m-o), enhancing trench curvatures (Figure 5) as predicted by Morra et al. (2009, 2012). Importantly, we find that this process occurs in the complex rheology slabs and mantle flow examined here, thus complementing results from the isoviscous slabs of Morra et al. (2009, 2012).

We found that within the parameter space investigated, the increased flexural stiffness of a spherical plate, which is expected to hinder plate deformation compared to a flat plate (Mahadevan et al., 2010), is not a significant factor. This would be expected to reduce along-strike variations in trench curvature, but we find the opposite, with the trench in the 4800 km-wide spherical case more curved (a difference of  $\sim 180$  km between

the points of most and least retreat) than that of the equivalent Cartesian case in the larger box ( $\sim 167$  km between the points of most and least retreat, Figure 5c). Although results have not been shown here, we find that these trends are consistent for cases with older plates (i.e., with a larger negative buoyancy and strength than our reference plates) in Chen et al. (2022). This implies that the along-strike buckling that occurs during slab descent in a spherical domain is a more important consideration, overcoming its elevated flexural stiffness. This is in agreement with Chamolly and Ribe (2021), who used scaling analyses in an axisymmetric thin viscous shell to show that the reduction of space with depth in a concentric sphere leads to compressional Hoop stresses that drive buckling instabilities. Chamolly and Ribe (2021) also showed that the stiffening effect of sphericity acts more strongly on smaller and shallower plates. However, they noted two major limitations of their study: (i) the model's axisymmetry limited subduction to occur solely via trench rollback, and prevented along-strike buckling of the plate; and (ii) the model neglected the free-slip boundary condition at Earth's core-mantle-boundary, which will influence the flow regime. Given these limitations, it is reassuring that the conclusions of our study about the effect of plate shape on flexural stiffness, in a truly spherical geometry with visco-plastic plates, are consistent.

We did not observe any substantial impact from the transition zone's curvature and its potential ability to enhance slab stagnation and trench retreat. As illustrated in Figure 1(c), the transition zone curves away from the descending slab at the point of impingement. The angle of interaction of a slab with the curved interface at depth is shallower by the angular distance,  $\theta$ , travelled by the slab tip, compared to a parallel slab that is in a Cartesian domain, where lateral movement of the slab tip does not affect the angle of incidence. Previous studies suggest that slab stagnation and trench retreat would be enhanced in spherical models as a result (e.g., Christensen, 2001; Torii & Yoshioka, 2007; Tagawa et al., 2007; Ribe, 2010), yet the spherical cases predict less trench retreat than their Cartesian counterparts in the larger box domain (Figure 4g-i). We suggest that the aforementioned increased slab sinking velocity and bending-mode behaviour of the subducting plate on a sphere has a more dominant affect on subduction dynamics and the dip of the slab tip as it descends in the upper mantle, thus the assumption in Figure 1(c) that the Cartesian and spherical models have the same slab dip prior to interacting with the transition zone is unlikely to be valid.

Overall, we find that Cartesian models provide a reasonable approximation of behaviour on a sphere for narrower plates and for qualitative analyses of subduction systems. However, when considering wider plates, such as those equal to or exceeding  $\sim 2400$  km in width, Cartesian models become less applicable, due to: (i) model dynamics being strongly affected by imposed sidewall boundary conditions, particularly in smaller Cartesian domains; (ii) their inability to capture the complexity of mantle flow generated by subduction in a finite spherical shell domain; and (iii) wider plates being more strongly influenced by buckling to adjust to Earth's sphericity during slab descent, a process that cannot be captured in Cartesian domains. It is worth emphasizing that our key results are consistent for older (i.e. stronger and denser) plates, where the spherical models also exhibit lower trench retreat velocities, greater along-strike curvature for wider slabs and higher sinking velocities, relative to their Cartesian counterparts. Given the computational cost of our simulations, we have been unable to precisely identify the width at which the effect of sphericity invalidates Cartesian models, and it would also be sensitive to slab properties such as age and width. Nonetheless, based on the simulations presented herein, we suggest that the sphericity cannot be overlooked for slabs of width  $\sim 2400$  km or above.

## 5 Implications for the Spatial and Temporal Evolution of Earth's Subduction Zones

Our analyses highlight the role of sphericity in influencing many of the primary features of Earth's subduction zones, such as the evolution of trench curvature and slab mor-



phology at depth. Although curved trenches are predicted in our Cartesian models (Figure 5), arising from toroidal flow around slab edges (e.g., Schellart, 2004; Funicello et al., 2006; Stegman et al., 2006; Schellart et al., 2007), the reduction of space with depth in spherical domains further enhances trench curvature and slab buckling during slab descent (Figure 6), and drives an increase in the lateral stresses associated with subducting slabs in a spherical domain (e.g., Fukao et al., 1987; Tanimoto, 1998; Yamaoka et al., 1986; Schettino & Tassi, 2012). Observations that support slab deformation to accommodate such a reduction in slab width include seismicity and seismic tomography in regions such as the Nazca, Farallon, and Sumatran subduction zones (e.g., Cahill & Isacks, 1992; Pesicek et al., 2008; Liu & Stegman, 2011; Hayes et al., 2018; van der Meer et al., 2018).

Our results suggest that Cartesian models, that are executed in domains where the distance between the plate and side boundaries is insufficient to allow for the free transport of material around the slab, limit trench retreat, even promoting trench advance at the centre of wider subducting plates (e.g., the C\_W4800 case). The more readily retreating trenches predicted in larger Cartesian or spherical domains will facilitate back-arc extension (e.g., Faccenna et al., 1996; Heuret et al., 2007; Nakakuki & Mura, 2013). Most existing studies that examined the role of plate width in modulating the dynamics of subduction were executed in domains of similar dimensions to our reference Cartesian cases (e.g., Stegman et al., 2006; Schellart et al., 2007; Stegman, Schellart, & Freeman, 2010; Schellart, 2017, 2020). The inferences drawn from such models have been applied to understanding the evolution of trench shape at several subduction zones, with a prominent example being the South American subduction zone and the formation of the Bolivian Orocline. Schellart (2017) propose that this orocline is principally the manifestation of the progressive evolution of a very wide subduction zone, while Schellart (2020) suggest that the formation of flat slabs in such wide and long-lived subduction zones could be facilitated by the slab centre resisting rollback. However, in the 6000 km-wide plate simulated in their studies, the oroclinal centre of the trench, upon which their key conclusions on trench curvature and flat slabs are based, is likely exaggerated. This is shown by the comparison of our reference case C\_W4800 (with similar plate to domain ratio) to S\_W4800 (Figure 5), where trench curvature in the Cartesian case is overestimated. Our spherical models confirm that plate width has an important role to play in retarding trench retreat at the centre of the subduction zone. However, given the prominence of curvature at the Bolivian Orocline and the tendency for Cartesian models in smaller domains to overestimate the significance of such features, it is likely that other factors have enhanced orocline formation and induced flat slab subduction along the Andean Trench. These factors may include trench parallel variations in slab age (e.g., Capitanio et al., 2011; Müller et al., 2016), interactions with a thick continental overriding plate (e.g., Clark et al., 2008; Bonnardot et al., 2008; Capitanio, Stegman, et al., 2010; van Dinther et al., 2010), and the subduction of buoyant anomalies (e.g., Gutscher et al., 1999; Mason et al., 2010; Suchoy et al., 2022).

Cartesian simulations of subduction have also been used to analyse how the presence of buoyant anomalies, such as oceanic plateaus and ridges, influences the evolution of subduction systems. It was found that trench motion was retarded in the region of buoyant features, pinning the trench in a cusp shape (e.g., Mason et al., 2010; Suchoy et al., 2022). Suchoy et al. (2022) investigated the subduction of buoyant anomalies with Cartesian numerical models using a similar setup to the C\_W2400 case analysed here, and found that their effect is dependent upon their location along the trench. When the buoyant ridge impinges at the centre of the trench, where trench motion is already hindered by plate width, trench retreat is further reduced locally, leading to significant along-strike variations in trench shape and locally reducing slab dip. Conversely, when the buoyant anomalies impinge on the trench in a region where it would want to retreat substantially (i.e., towards slab edges), they have less of an influence on the evolution of trench shape and slab dip. Our spherical models also exhibit along-strike variations in trench

retreat for wider plates, hence the qualitative conclusions from Suchoy et al. (2022) remain valid. However, our C\_W2400 case predicted a more significant reduction in trench retreat at the centre compared to the S\_W2400 case, suggesting that modelled trench shape variations due to the location of buoyant anomalies may be exaggerated in the smaller Cartesian domains.

Our models demonstrate that the flow field generated by wider slabs on a sphere not only elevate velocities in directly-adjacent mantle, but also have farther reaching effects. In the 4800-km wide spherical model, the subducting slab drives flow throughout the computational domain, which compares to a more localised flow field in the S\_W1200 case (Figure 7). The dynamics predicted in the ‘Big’ 4800 km-wide Cartesian case, executed in a domain of full width (mirrored at the symmetry plane) that exceeds Earth’s circumference, are also distinct from the equivalent spherical case, particularly when examining trench motion and trench shape diagnostics. These differences indicate that the flow field generated by large plates can influence not only nearby subduction systems, but also dynamics elsewhere within the mantle, through feedbacks modulated by the spherical geometry that are not captured in larger Cartesian domains. The interaction between slabs in double subduction systems, either facing (e.g., Cocos and Antilles) or opposing each other (e.g., Izu–Bonin–Marianas and Ryukyu) or adjacent with opposing convergence (e.g., Ryukyu–Manila or Alpine–Apennine trenches) has been shown by many studies in Cartesian boxes to be strongly affected by flow around the slab (e.g., Yamato et al., 2009; Čížková & Bina, 2015; Király et al., 2017; Holt et al., 2017, 2018; Peral et al., 2020). When such double systems, or the distances between two systems, reach length scales that exceed  $\sim 2400$  km, we expect that the effects of sphericity on the flow field will influence how the two subduction systems interact. On an even greater scale, as advocated by a number of previous studies (e.g., Becker & Faccenna, 2011; Matthews et al., 2012; Müller et al., 2016), our results demonstrate that large subduction systems on Earth, such as those associated with closure of the former Tethys ocean, or the present-day South American subduction zone, have the potential to strongly modulate global mantle flow, influencing the evolution of subduction zones in other parts of the globe, and potentially contributing towards global scale plate reorganisation events.

Taken together, our results demonstrate that spherical models are important to understand Earth’s subduction zones because: (i) they replicate the geometry of Earth’s mantle and do not include artificial side boundary conditions which alter the flow regime at and adjacent to subduction systems; (ii) they replicate the finite dimensions of Earth’s mantle, which facilitates a more realistic representation of feedback between mantle flow and subduction dynamics and will underpin future investigations into potential interactions between the flow field of different subduction zones; and (iii) they capture other geometric effects of Earth’s sphericity, including the reduction of space with depth and a radial gravity direction, which we have shown significantly impact the evolution of subduction systems.

## 6 Conclusions

We have presented a set of comparable multi-material composite-rheology free subduction models in 3-D Cartesian and spherical shell domains. With these, we have examined the role of sphericity in dictating the dynamics of subduction, also highlighting the limitations of Cartesian models and the sensitivity of their predictions to domain size. We find that the modes of subduction predicted by Cartesian models, particularly those in larger domains and for narrower slabs, are similar to their spherical counterparts. However, there are significant quantitative discrepancies between spherical and Cartesian models and these increase with increasing plate width.

Cartesian model results are strongly affected by box size, particularly as slab widths increase. This is because the mechanical boundary conditions imposed on sidewalls (which

do not exist within Earth’s mantle) influence the flow field, modifying material transport around the slab and, hence, trench retreat velocities, sinking velocities, and the evolution of the subduction system in general. The inferences drawn from some existing Cartesian based studies must therefore be considered in light of these limitations, including those that have examined the role of slab width in dictating the dynamics of subduction and the evolution of trench shape. Whilst this shortcoming can partially be overcome using larger computational domains (or imposing open or infinite sidewall boundary conditions), this fails to capture the complexity of mantle flow generated by subduction in a finite domain such as Earth’s mantle, particularly as plates get wider. Indeed, when the dimensions of Cartesian boxes exceed the dimensions of Earth’s mantle, simulations overestimate trench retreat, resulting in different slab morphologies and trench shapes.

There is an additional irreconcilable difference between Cartesian and spherical models: the reduction of space with depth in spherical shells, alongside the radial gravity direction, the effects of which cannot be captured in Cartesian domains, thus limiting their applicability. This reduction in space enhances along-strike buckling, trench curvature, and sinking velocities in spherical domains, with discrepancies between Cartesian and spherical models becoming more prominent for wider slabs. We find that the increased flexural stiffness of a spherical plate, which is expected to hinder plate deformation, is overshadowed by the slab buckling required to accommodate the reduction in space as the slab descends into deeper mantle, under the conditions considered herein. As a result, spherical models predict more deformed trenches than comparable Cartesian models, provided the latter are executed in domains of sufficient size.

In conclusion, our results suggest that Cartesian models are suitable for basic qualitative analyses of subduction style, particularly for narrower plates. However, sphericity must be considered for accurate quantitative analyses of Earth’s subduction systems, and is vital when investigating slabs at, or exceeding,  $\sim 2400$  km in width: at these scales, the effects of sphericity are too large to ignore.

## Open Research

The Fluidity computational modelling framework, including source code and documentation, is available from <https://fluidityproject.github.io/>; the version used for the simulations presented herein has been archived at Kramer, Wilson, et al. (2021). The input files required to reproduce the simulations presented herein have also been made available at Chen (2022). Figures have been prepared using Matplotlib, Cartopy and Paraview.

## Acknowledgments

F.C. is funded by an Australian Government Research Training Program (RTP) Scholarship. D.R.D. and S.C.K. acknowledge support from the Australian Research Council (ARC) under DP170100058, the Australian Research Data Commons (ARDC, under the G-Adopt platform grant: PL031), AuScope, Geosciences Australia and the National Computational Infrastructure (NCI). L.S. was funded by an EPSRC DTP studentship (EP/N509486/1), S.G. received support under NERC grant NE/K010743/1. This research was supported by the Australian Government’s National Collaborative Research Infrastructure Strategy (NCRIS), with access to computational resources provided on Gadi through the National Computational Merit Allocation Scheme and the ANU Merit Allocation Scheme. Authors would like to thank Cian Wilson, Chris Matthews, Thomas Duvernay, Siavash Ghelichkhan and Angus Gibson for fruitful discussions at various stages of this research.



## References

- Agrusta, R., Goes, S., & van Hunen, J. (2017). Subducting-slab transition-zone interaction: Stagnation, penetration and mode switches. *Earth and Planetary Science Letters*, 464, 10–23.
- Alsaif, M., Garel, F., Gueydan, F., & Davies, D. R. (2020). Upper plate deformation and trench retreat modulated by subduction-driven shallow asthenospheric flows. *Earth and Planetary Science Letters*, 532, 116013.
- Balay, S., Abhyankar, S., Adams, M. F., Brown, J., Brune, P., Buschelman, K., ... Zhang, H. (2021a). *PETSc users manual* (Tech. Rep. No. ANL-95/11 - Revision 3.15). Argonne National Laboratory. Retrieved from <https://www.mcs.anl.gov/petsc>
- Balay, S., Abhyankar, S., Adams, M. F., Brown, J., Brune, P., Buschelman, K., ... Zhang, H. (2021b). *PETSc Web page*. <https://www.mcs.anl.gov/petsc>. Retrieved from <https://www.mcs.anl.gov/petsc>
- Balay, S., Gropp, W. D., McInnes, L. C., & Smith, B. F. (1997). Efficient management of parallelism in object-oriented numerical software libraries. In *Modern software tools for scientific computing* (pp. 163–202). Birkhauser Boston Inc.
- Bayly, B. (1982). Geometry of subducted plates and island arcs viewed as a buckling problem. *Geology*, 10(12), 629–632.
- Beall, A., Fagereng, Å., Davies, J. H., Garel, F., & Davies, D. R. (2021). Influence of subduction zone dynamics on interface shear stress and potential relationship with seismogenic behavior. *Geochemistry, Geophysics, Geosystems*, 22(2), e2020GC009267.
- Becker, T. W., & Faccenna, C. (2011). Mantle conveyor beneath the tethyan collisional belt. *Earth and Planetary Science Letters*, 310(3–4), 453–461.
- Bellahsen, N., Faccenna, C., & Funiciello, F. (2005). Dynamics of subduction and plate motion in laboratory experiments: Insights into the “plate tectonics” behavior of the Earth. *Journal of Geophysical Research: Solid Earth*, 110(B1).
- Bonnardot, M.-A., Hassani, R., Tric, E., Ruellan, E., & Régnier, M. (2008). Effect of margin curvature on plate deformation in a 3-d numerical model of subduction zones. *Geophysical Journal International*, 173(3), 1084–1094.
- Bower, D. J., Gurnis, M., & Seton, M. (2013). Lower mantle structure from paleogeographically constrained dynamic Earth models. *Geochem. Geophys. Geosys.*, 14, 44–63. doi: 10.1029/2012GC004267
- Cahill, T., & Isacks, B. L. (1992). Seismicity and shape of the subducted nazca plate. *Journal of Geophysical Research: Solid Earth*, 97(B12), 17503–17529.
- Capitanio, F. A., Faccenna, C., Zlotnik, S., & Stegman, D. R. (2011). Subduction dynamics and the origin of Andean orogeny and the Bolivian orocline. *Nature*, 480(7375), 83–86.
- Capitanio, F. A., Morra, G., & Goes, S. (2007). Dynamic models of downgoing plate-buoyancy driven subduction: Subduction motions and energy dissipation. *Earth and Planetary Science Letters*, 262(1–2), 284–297.
- Capitanio, F. A., Stegman, D. R., Moresi, L. N., & Sharples, W. (2010). Upper plate controls on deep subduction, trench migrations and deformations at convergent margins. *Tectonophysics*, 483(1–2), 80–92.
- Capitanio, F. A., Zlotnik, S., & Faccenna, C. (2010). Controls on subduction reorganization in the hellenic margin, eastern mediterranean. *Geophysical research letters*, 37(14).
- Cerpa, N. G., Sigloch, K., Garel, F., Heuret, A., Davies, D. R., & Mihalynuk, M. (2022). The effect of a weak asthenospheric layer on surface kinematics, subduction dynamics and slab morphology in the lower mantle. *J. Geophys. Res.*, 127, e2022JB024494. doi: 10.1029/2022JB024494
- Chamolly, A., & Ribe, N. M. (2021). Fluid mechanics of free subduction on a sphere. part 1. the axisymmetric case. *Journal of Fluid Mechanics*, 929.

- Chen, F. (2022). *cfq2738/Comparing-the-Dynamics-of-Free-Subduction- in-Cartesian-and-Spherical-Domains: Submission to Geochemistry, Geophysics, Geosystems*. Zenodo. Retrieved from <https://doi.org/10.5281/zenodo.7220616> doi: 10.5281/zenodo.7220616
- Chen, F., Davies, D. R., Goes, S., Suchoy, L., & Kramer, S. C. (2022). How slab age and width combine to dictate the dynamics and evolution of subduction systems: a 3-d spherical study. *Earth and Space Science Open Archive*, 29. Retrieved from <https://doi.org/10.1002/essoar.10511804.1> doi: 10.1002/essoar.10511804.1
- Chertova, M. V., Geenen, T., Van Den Berg, A., & Spakman, W. (2012). Using open sidewalls for modelling self-consistent lithosphere subduction dynamics. *Solid Earth*, 3(2), 313–326.
- Chertova, M. V., Spakman, W., & Steinberger, B. (2018). Mantle flow influence on subduction evolution. *Earth and Planetary Science Letters*, 489, 258–266.
- Christensen, U. (2001). Geodynamic models of deep subduction. *Physics of the Earth and Planetary Interiors*, 127(1-4), 25–34.
- Čížková, H., & Bina, C. R. (2015). Geodynamics of trench advance: Insights from a philippine-sea-style geometry. *Earth and Planetary Science Letters*, 430, 408–415.
- Čížková, H., van den Berg, A. P., Spakman, W., & Matyska, C. (2012). The viscosity of earth’s lower mantle inferred from sinking speed of subducted lithosphere. *Physics of the earth and Planetary Interiors*, 200, 56–62.
- Čížková, H., van Hunen, J., & van den Berg, A. (2007). Stress distribution within subducting slabs and their deformation in the transition zone. *Physics of the Earth and Planetary Interiors*, 161(3-4), 202–214.
- Čížková, H., van Hunen, J., van den Berg, A. P., & Vlaar, N. J. (2002). The influence of rheological weakening and yield stress on the interaction of slabs with the 670 km discontinuity. *Earth and Planetary Science Letters*, 199(3-4), 447–457.
- Clark, S. R., Stegman, D., & Müller, R. D. (2008). Episodicity in back-arc tectonic regimes. *Physics of the Earth and Planetary Interiors*, 171(1-4), 265–279.
- Davies, D. R., Goes, S., & Lau, H. C. P. (2015). Thermally Dominated Deep Mantle LLSVPs: A Review. In A. Khan & F. Deschamps (Eds.), *The Earth’s Heterogeneous Mantle* (p. 441-477). Springer International Publishing. doi: 10.1007/978-3-319-15627-9\_14
- Davies, D. R., Goes, S., & Sambridge, M. (2015). On the relationship between volcanic hotspot locations, the reconstructed eruption sites of large igneous provinces and deep mantle seismic structure. *Earth Planet. Sci. Lett.*, 411, 121–130. doi: 10.1016/j.epsl.2014.11.052
- Davies, D. R., Le Voci, G., Goes, S., Kramer, S. C., & Wilson, C. R. (2016). The mantle wedge’s transient 3-D flow regime and thermal structure. *Geochem. Geophys. Geosys.*, 17, 78-100. doi: 10.1002/2015GC006125
- Davies, D. R., Wilson, C. R., & Kramer, S. C. (2011). Fluidity: A fully unstructured anisotropic adaptive mesh computational modeling framework for geodynamics. *Geochemistry, Geophysics, Geosystems*, 12(6).
- Duretz, T., Gerya, T. V., & May, D. A. (2011). Numerical modelling of spontaneous slab breakoff and subsequent topographic response. *Tectonophysics*, 502(1-2), 244–256.
- Duretz, T., Schmalholz, S., & Gerya, T. (2012). Dynamics of slab detachment. *Geochemistry, Geophysics, Geosystems*, 13(3).
- Enns, A., Becker, T. W., & Schmeling, H. (2005). The dynamics of subduction and trench migration for viscosity stratification. *Geophysical Journal International*, 160(2), 761–775.
- Faccenna, C., Davy, P., Brun, J.-P., Funiciello, R., Giardini, D., Mattei, M., & Nalpas, T. (1996). The dynamics of back-arc extension: an experimental approach

- to the opening of the tyrrhenian sea. *Geophysical Journal International*, 126(3), 781–795.
- Forsyth, D., & Uyeda, S. (1975). On the relative importance of the driving forces of plate motion. *Geophysical Journal International*, 43(1), 163–200.
- Frank, F. (1968). Curvature of island arcs. *Nature*, 220(5165), 363–363.
- Fukao, Y., Yamaoka, K., & Sakurai, T. (1987). Spherical shell tectonics: buckling of subducting lithosphere. *Physics of the earth and planetary interiors*, 45(1), 59–67.
- Funiciello, F., Moroni, M., Piromallo, C., Faccenna, C., Cenedese, A., & Bui, H. A. (2006). Mapping mantle flow during retreating subduction: Laboratory models analyzed by feature tracking. *Journal of Geophysical Research: Solid Earth*, 111(B3).
- Garel, F., Goes, S., Davies, D. R., Davies, J. H., Kramer, S. C., & Wilson, C. R. (2014). Interaction of subducted slabs with the mantle transition-zone: A regime diagram from 2-D thermo-mechanical models with a mobile trench and an overriding plate. *Geochemistry, Geophysics, Geosystems*, 15(5), 1739–1765.
- Goes, S., Agrusta, R., van Hunen, J., & Garel, F. (2017). Subduction-transition zone interaction: A review. *Geosphere*, 13(3), 644–664.
- Gurnis, M., & Hager, B. H. (1988). Controls of the structure of subducted slabs. *Nature*, 335(6188), 317–321.
- Gutscher, M. A., Olivet, J. L., Aslanian, D., Eissen, J. P., & Maury, R. (1999). The “lost Inca Plateau”: Cause of flat subduction beneath Peru? *Earth and Planetary Science Letters*, 171(3), 335–341.
- Han, L., & Gurnis, M. (1999). How valid are dynamic models of subduction and convection when plate motions are prescribed? *Physics of the Earth and Planetary Interiors*, 110(3-4), 235–246.
- Hassan, R., Müller, R. D., Gurnis, M., Williams, S. E., & Flament, N. (2016). A rapid burst in hotspot motion through the interaction of tectonics and deep mantle flow. *Nature*, 533(7602), 239–242.
- Hayes, G. P., Moore, G. L., Portner, D. E., Hearne, M., Flamme, H., Furtney, M., & Smoczyk, G. M. (2018). Slab2, a comprehensive subduction zone geometry model. *Science*, 362(6410), 58–61.
- Heuret, A., Funiciello, F., Faccenna, C., & Lallemand, S. (2007). Plate kinematics, slab shape and back-arc stress: A comparison between laboratory models and current subduction zones. *Earth and Planetary Science Letters*, 256(3-4), 473–483.
- Holt, A. F., & Royden, L. H. (2020). Subduction dynamics and mantle pressure: 2. towards a global understanding of slab dip and upper mantle circulation. *Geochemistry, Geophysics, Geosystems*, 21(7), e2019GC008771.
- Holt, A. F., Royden, L. H., & Becker, T. W. (2017). The dynamics of double slab subduction. *Geophysical Journal International*, 209(1), 250–265.
- Holt, A. F., Royden, L. H., Becker, T. W., & Faccenna, C. (2018). Slab interactions in 3-d subduction settings: The philippine sea plate region. *Earth and Planetary Science Letters*, 489, 72–83.
- Ishizuka, O., Tani, K., Reagan, M. K., Kanayama, K., Umino, S., Harigane, Y., . . . Dunkley, D. J. (2011). The timescales of subduction initiation and subsequent evolution of an oceanic island arc. *Earth and Planetary Science Letters*, 306(3-4), 229–240.
- Jarrard, R. D. (1986). Relations among subduction parameters. *Reviews of Geophysics*, 24(2), 217–284.
- Király, A., Capitanio, F. A., Funiciello, F., & Faccenna, C. (2017). Subduction induced mantle flow: Length-scales and orientation of the toroidal cell. *Earth and Planetary Science Letters*, 479, 284–297.
- Kramer, S. C., Davies, D. R., & Wilson, C. R. (2021). Analytical solutions for mantle flow in cylindrical and spherical shells. *Geoscientific Model Development*,

- 14(4), 1899–1919.
- Kramer, S. C., Wilson, C., Funke, S. W., Greaves, T., Avdis, A., Davies, R., . . .  
Ham, D. A. (2021). *FluidityStokes/fluidity: Spherical Adaptivity branch*.  
Zenodo. Retrieved from <https://doi.org/10.5281/zenodo.5636819> doi:  
10.5281/zenodo.5636819
- Kramer, S. C., Wilson, C. R., & Davies, D. R. (2012). An implicit free surface algo-  
rithm for geodynamical simulations. *Physics of the Earth and Planetary Interi-  
ors*, 194, 25–37.
- Lallemant, S., Heuret, A., & Boutelier, D. (2005). On the relationships between  
slab dip, back-arc stress, upper plate absolute motion, and crustal nature in  
subduction zones. *Geochemistry, Geophysics, Geosystems*, 6(9).
- Laravie, J. A. (1975). Geometry and lateral strain of subducted plates in island arcs.  
*Geology*, 3(9), 484–486.
- Le Voci, G., Davies, D. R., Goes, S., Kramer, S. C., & Wilson, C. R. (2014).  
A systematic 2-D investigation into the mantle wedge’s transient flow  
regime and thermal structure: complexities arising from a hydrated rheol-  
ogy and thermal buoyancy. *Geochem. Geophys. Geosys.*, 15, 28–51. doi:  
10.1002/2013GC005022
- Li, Z.-H., & Ribe, N. M. (2012). Dynamics of free subduction from 3-d boundary el-  
ement modeling. *Journal of Geophysical Research: Solid Earth*, 117(B6).
- Lithgow-Bertelloni, C., & Richards, M. A. (1998). The dynamics of Cenozoic and  
Mesozoic plate motions. *Reviews of Geophysics*, 36(1), 27–78.
- Liu, L., & Stegman, D. R. (2011). Segmentation of the farallon slab. *Earth and  
Planetary Science Letters*, 311(1-2), 1–10.
- Mahadevan, L., Bendick, R., & Liang, H. (2010). Why subduction zones are curved.  
*Tectonics*, 29(6).
- Martinod, J., Funiciello, F., Faccenna, C., Labanieh, S., & Regard, V. (2005). Dy-  
namical effects of subducting ridges: insights from 3-D laboratory models.  
*Geophysical Journal International*, 163(3), 1137–1150.
- Mason, W. G., Moresi, L., Betts, P. G., & Miller, M. S. (2010). Three-dimensional  
numerical models of the influence of a buoyant oceanic plateau on subduction  
zones. *Tectonophysics*, 483(1-2), 71–79.
- Matthews, K. J., Seton, M., & Müller, R. D. (2012). A global-scale plate reorga-  
nization event at 105–100 ma. *Earth and Planetary Science Letters*, 355, 283–  
298.
- Mériaux, C. A., May, D. A., Mansour, J., Chen, Z., & Kaluza, O. (2018). Bench-  
mark of three-dimensional numerical models of subduction against a labora-  
tory experiment. *Physics of the Earth and Planetary Interiors*, 283, 110–121.
- Miller, M. S., Gorbato, A., & Kennett, B. L. (2006). Three-dimensional visualiza-  
tion of a near-vertical slab tear beneath the southern mariana arc. *Geochem-  
istry, Geophysics, Geosystems*, 7(6).
- Morra, G., Chatelain, P., Tackley, P., & Koumoutsakos, P. (2007). Large scale three-  
dimensional boundary element simulation of subduction. In *International con-  
ference on computational science* (pp. 1122–1129).
- Morra, G., Chatelain, P., Tackley, P., & Koumoutsakos, P. (2009). Earth curvature  
effects on subduction morphology: Modeling subduction in a spherical setting.  
*Acta Geotechnica*, 4(2), 95–105.
- Morra, G., Quevedo, L., & Müller, R. D. (2012). Spherical dynamic models of top-  
down tectonics. *Geochemistry, Geophysics, Geosystems*, 13(3).
- Müller, R. D., Seton, M., Zahirovic, S., Williams, S. E., Matthews, K. J., Wright,  
N. M., . . . Cannon, J. (2016). Ocean basin evolution and global-scale plate  
reorganization events since Pangea breakup. *Annual Review of Earth and  
Planetary Sciences*, 44, 107–138.
- Nakakuki, T., & Mura, E. (2013). Dynamics of slab rollback and induced back-arc  
basin formation. *Earth and Planetary Science Letters*, 361, 287–297.

- OzBench, M., Regenauer-Lieb, K., Stegman, D. R., Morra, G., Farrington, R., Hale, A., ... Moresi, L. (2008). A model comparison study of large-scale mantle–lithosphere dynamics driven by subduction. *Physics of the Earth and Planetary Interiors*, 171(1-4), 224–234.
- O’Brien, P. J. (2001). Subduction followed by collision: Alpine and himalayan examples. *Physics of the Earth and Planetary Interiors*, 127(1-4), 277–291.
- Peral, M., Ruh, J., Zlotnik, S., Funiciello, F., Fernandez, M., Vergés, J., & Gerya, T. (2020). Analog and numerical experiments of double subduction systems with opposite polarity in adjacent segments. *Geochemistry, Geophysics, Geosystems*, 21(6), e2020GC009035.
- Perrin, A., Goes, S., Prytulak, J., Rondenay, S., & Davies, D. R. (2018). Mantle wedge temperatures and their potential relation to volcanic arc location. *Earth and Planetary Science Letters*, 501, 67–77.
- Pesicek, J., Thurber, C., Widiyantoro, S., Engdahl, E., & DeShon, H. (2008). Complex slab subduction beneath northern sumatra. *Geophysical Research Letters*, 35(20).
- Piromallo, C., Becker, T., Funiciello, F., & Faccenna, C. (2006). Three-dimensional instantaneous mantle flow induced by subduction. *Geophysical Research Letters*, 33(8).
- Pozrikidis, C. (1992). *Boundary integral and singularity methods for linearized viscous flow*. Cambridge university press.
- Pysklywec, R. N., Beaumont, C., & Fullsack, P. (2000). Modeling the behavior of the continental mantle lithosphere during plate convergence. *Geology*, 28(7), 655–658.
- Quinquis, M. E., Buitter, S. J., & Ellis, S. (2011). The role of boundary conditions in numerical models of subduction zone dynamics. *Tectonophysics*, 497(1-4), 57–70.
- Ribe, N. M. (2010). Bending mechanics and mode selection in free subduction: A thin-sheet analysis. *Geophysical Journal International*, 180(2), 559–576.
- Rosenbaum, G., Giles, D., Saxon, M., Betts, P. G., Weinberg, R. F., & Duboz, C. (2005). Subduction of the nazca ridge and the inca plateau: Insights into the formation of ore deposits in peru. *Earth and Planetary Science Letters*, 239(1-2), 18–32.
- Royden, L. H., & Holt, A. F. (2020). Subduction dynamics and mantle pressure: 1. an analytical framework relating subduction geometry, plate motion, and asthenospheric pressure: 1. an analytical framework relating subduction geometry, plate motion, and asthenospheric pressure. *Geochemistry, Geophysics, Geosystems*, 21(7), e2020GC009032.
- Rubey, M., Brune, S., Heine, C., Davies, D. R., Williams, S. E., & Müller, R. D. (2017). Global patterns in Earth’s dynamic topography since the Jurassic: the role of subducted slabs. *Solid Earth*, 8, 899-919. doi: 10.5194/se-8-899-2017
- Schellart, W. P. (2004). Kinematics of subduction and subduction-induced flow in the upper mantle. *Journal of Geophysical Research: Solid Earth*, 109(B7).
- Schellart, W. P. (2017). Andean mountain building and magmatic arc migration driven by subduction-induced whole mantle flow. *Nature communications*, 8(1), 1–13.
- Schellart, W. P. (2020). Control of subduction zone age and size on flat slab subduction. *Frontiers in Earth Science*, 8, 26.
- Schellart, W. P., Freeman, J., Stegman, D. R., Moresi, L., & May, D. (2007). Evolution and diversity of subduction zones controlled by slab width. *Nature*, 446(7133), 308–311.
- Schellart, W. P., & Strak, V. (2021). Geodynamic models of short-lived, long-lived and periodic flat slab subduction. *Geophysical Journal International*, 226(3), 1517–1541.
- Schettino, A., & Tassi, L. (2012). Trench curvature and deformation of the subduct-



- ing lithosphere. *Geophysical Journal International*, 188(1), 18–34.
- Schmeling, H., Babeyko, A., Enns, A., Faccenna, C., Funiciello, F., Gerya, T., ... others (2008). A benchmark comparison of spontaneous subduction models—towards a free surface. *Physics of the Earth and Planetary Interiors*, 171(1-4), 198–223.
- Scholz, C., & Page, R. (1970). Buckling in island arcs. In *Transactions-american geophysical union* (Vol. 51, p. 429).
- Stegman, D. R., Farrington, R., Capitanio, F. A., & Schellart, W. P. (2010). A regime diagram for subduction styles from 3-D numerical models of free subduction. *Tectonophysics*, 483(1-2), 29–45.
- Stegman, D. R., Freeman, J., Schellart, W. P., Moresi, L., & May, D. (2006). Influence of trench width on subduction hinge retreat rates in 3-D models of slab rollback. *Geochemistry, Geophysics, Geosystems*, 7(3).
- Stegman, D. R., Schellart, W. P., & Freeman, J. (2010). Competing influences of plate width and far-field boundary conditions on trench migration and morphology of subducted slabs in the upper mantle. *Tectonophysics*, 483(1-2), 46–57.
- Stern, R. J. (2002). Subduction zones. *Reviews of geophysics*, 40(4), 3–1.
- Strak, V., & Schellart, W. P. (2016). Control of slab width on subduction-induced upper mantle flow and associated upwellings: Insights from analog models. *Journal of Geophysical Research: Solid Earth*, 121(6), 4641–4654.
- Strobach, K. (1973). Curvature of island arcs and plate tectonics. *Z. Geophys*, 39, 819–831.
- Suchoy, L., Goes, S., Chen, F., & Davies, R. (2022). How aseismic ridges modify the dynamics of free subduction: a 3-d numerical investigation. *Frontiers in Earth Science*, 611.
- Suchoy, L., Goes, S., Maunder, B., Garel, F., & Davies, R. (2021). Effects of basal drag on subduction dynamics from 2d numerical models. *Solid Earth*, 12(1), 79–93.
- Tagawa, M., Nakakuki, T., & Tajima, F. (2007). Dynamical modeling of trench retreat driven by the slab interaction with the mantle transition zone. *Earth, planets and space*, 59(2), 65–74.
- Tanimoto, T. (1998). State of stress within a bending spherical shell and its implications for subducting lithosphere. *Geophysical Journal International*, 134(1), 199–206.
- Torii, Y., & Yoshioka, S. (2007). Physical conditions producing slab stagnation: Constraints of the Clapeyron slope, mantle viscosity, trench retreat, and dip angles. *Tectonophysics*, 445(3-4), 200–209.
- Tosi, N., Stein, C., Noack, L., Hüttig, C., Maierová, P., Samuel, H., ... Tackley, P. J. (2015). A community benchmark for viscoplastic thermal convection in a 2-d square box. *Geochemistry, Geophysics, Geosystems*, 16(7), 2175–2196. doi: 10.1002/2015GC005807
- van der Meer, D. G., van Hinsbergen, D. J., & Spakman, W. (2018). Atlas of the underworld: Slab remnants in the mantle, their sinking history, and a new outlook on lower mantle viscosity. *Tectonophysics*, 723, 309–448.
- van Dinther, Y., Morra, G., Funiciello, F., & Faccenna, C. (2010). Role of the overriding plate in the subduction process: Insights from numerical models. *Tectonophysics*, 484(1-4), 74–86.
- Wang, K., Hu, Y., & He, J. (2012). Deformation cycles of subduction earthquakes in a viscoelastic earth. *Nature*, 484(7394), 327–332.
- Wilson, C. R. (2009). *Modelling multiple-material flows on adaptive unstructured meshes*. PhD Thesis, Imperial College London, UK.
- Yamaoka, K. (1988). Spherical shell tectonics: on the buckling of the lithosphere at subduction zones. *Tectonophysics*, 147(3-4), 179–191.
- Yamaoka, K., Fukao, Y., & Kumazawa, M. (1986). Spherical shell tectonics: Effects

- 977 of sphericity and inextensibility on the geometry of the descending lithosphere.  
 978 *Reviews of Geophysics*, 24(1), 27–53.
- 979 Yamato, P., Husson, L., Braun, J., Loiselet, C., & Thieulot, C. (2009). Influence of  
 980 surrounding plates on 3d subduction dynamics. *Geophysical Research Letters*,  
 981 36(7).
- 982 Yuan, X., Sobolev, S. V., Kind, R., Oncken, O., Bock, G., Asch, G., . . . others  
 983 (2000). Subduction and collision processes in the central andes constrained by  
 984 converted seismic phases. *Nature*, 408(6815), 958–961.